

Temperature Extrapolation of Henry's Law Constants and the Isothermic Heat of Adsorption

Daniel W. Siderius,^{*,†,‡} Harold W. Hatch,[†] and Vincent K. Shen[†]

[†]*Chemical Sciences Division, National Institute of Standards and Technology,
Gaithersburg, Maryland 20899-8320, United States*

[‡]*Corresponding Author*

E-mail: daniel.siderius@nist.gov

Abstract

Computational screening of adsorbent materials often uses the Henry’s law constant (K_H) (at a particular temperature) as a first discriminator metric due to its relative ease of calculation. The isosteric heat of adsorption in the limit of zero pressure (q_{st}^∞) is often calculated along with the Henry’s law constant, and both properties are informative metrics of adsorbent material performance at low-pressure conditions. In this article, we introduce a method for extrapolating K_H as a function of temperature, using series-expansion coefficients that are easily computed at the same time as K_H itself; the extrapolation function also yields q_{st}^∞ . The extrapolation is highly accurate over a wide range of temperatures when the basis temperature is sufficiently high, for a wide range of adsorbent materials and adsorbate gases. Various results suggest that the extrapolation is accurate when the extrapolation range in inverse-temperature space is limited to $|\beta - \beta_0| < 0.5$ mol/kJ. Application of the extrapolation to a large set of materials is shown to be successful provided that K_H is not extremely large and/or the extrapolation coefficients converge satisfactorily. The extrapolation is also able to predict q_{st}^∞ for a system that shows an unusually large temperature dependence. The work provides a robust method for predicting K_H and q_{st}^∞ over a wide range of industrially relevant temperatures with minimal effort beyond that necessary to compute those properties at a single temperature, which facilitates the addition of practical operating (or processing) conditions to computational screening exercises.

1 Introduction

Separations are a large energy expense in the chemical sector, accounting for nearly 40 % of total energy consumption related to production of certain chemicals in the USA, primarily through thermal processes (e.g., distillation, drying, extraction, etc.)¹ Additionally, chemical separations may account for as much as 10 % to 15 % of total energy consumption in the USA.² As such, reducing energy consumption related to chemical separations is viewed as a prime option for increasing energy efficiency at a whole-economy scale.³ Questions of chemical separations also intersect with concerns of carbon dioxide emissions, since improvements in energy efficiency would likely reduce those emissions, and carbon dioxide capture (from either an effluent stream or directly from the atmosphere) is itself a chemical separation.

Adsorbent materials are viewed as an important platform technology for reducing energy consumption in chemical separations due to lower thermal demands of adsorption-driven separations² as well as their use in adjacent applications such as gas storage,⁴ chemical sensing,⁵ and drug delivery.⁶ Unfortunately, the process of designing, synthesizing, and manufacturing an adsorbent to achieve a particular chemical separation remains largely empirically based, which is costly and inefficient. Thus, separation scientists often resort to investigating materials that have already been synthesized and studied in the literature. A primary challenge is therefore the identification of favorable materials for a particular application of adsorption, which is only complicated by the rapid pace at which new adsorbent materials are developed or identified. Candidate materials include metal-organic frameworks (MOFs),⁷ zeolites,⁸ covalent-organic frameworks,⁹ polymers of intrinsic microporosity,¹⁰ etc. Each class of materials offers advantages and disadvantages, such as nearly-infinite chemical diversity, tunable pore sizes and shapes, material resiliency, and material price, with a unifying theme being the overwhelming number of possible materials.¹¹ In response to this challenge, computational screening of adsorbent materials has emerged as a widespread tool for sorting and identifying promising materials as a precursor to experimental synthesis and evaluation.¹² Furthermore, computational screening and hypothetical material evolution has been facili-

tated by the compilation and development of large databases of adsorbent materials^{13–15} and regular improvement of molecular-level analysis tools for computational evaluation of those materials.^{16,17}

Computational screening of adsorbents typically uses a series of progressively more computationally expensive metrics or features to discriminate between adsorbents.¹⁴ After the simplest geometric descriptors of adsorbents (e.g., surface area, pore volume, etc.) that are independent of both the adsorptive species and process conditions, the first “chemical” descriptor used to evaluate adsorbent material performance is often the Henry’s law constant of a material, as it also depends on the adsorptive identity and temperature but is yet a simple and fast calculation.¹⁸ The Henry’s law constant may also estimate the selectivity of a material toward specific chemicals, since the ratio of Henry’s law constants of two species for a particular material at one temperature is equal to the selectivity ratio of those chemicals in the limit of zero pressure.¹⁹ Beyond the Henry’s law constant, full molecular simulations²⁰ or machine-learning approaches²¹ may also inform screening exercises targeting more realistic conditions.

More recently, thermodynamic extrapolation has emerged as a tool for estimating the variation of thermophysical properties with some imposed condition (e.g., temperature, pressure, or volume), by combining molecular simulation results with careful exploitation of statistical mechanics.^{22–27} Briefly, the approach is based on determining analytic expressions for the derivatives of an observable quantity (e.g., average potential energy, macrostate probability, etc.) with respect to a constraint variable (e.g., temperature); those derivatives are useful when they are analytic functions of other observables. A Taylor series is then used to estimate the original observable as a function of the constraint variable. For example, Mahynski et al. used this approach to reproduce the entire vapor-liquid phase diagram of the Lennard-Jones fluid from a single grand canonical transition-matrix Monte Carlo (MC) simulation at a supercritical temperature.²² Thermodynamic extrapolation has shown great promise for extending the impact of individual molecular simulations beyond the original

simulation conditions.

In the present work, we apply the concepts of thermodynamic extrapolation to the Henry’s law constant and isosteric heat for adsorption systems, with the objective of yielding an accurate estimate of those properties as a function of arbitrary temperature. The first-order variation of the Henry’s law constant with temperature is ostensibly known from the isosteric heat of adsorption. We show how higher-order derivatives are easily computed from moments of the adsorbate-adsorbent potential energy, which yields highly accurate series extrapolations for the Henry’s law constant and the isosteric heat. The extrapolations offer the option to extend adsorbent material screening exercises in temperature space, with minimal additional computational effort.

This paper is organized as follows. In Section 2, we briefly present the statistical mechanical basis for computation of the Henry’s law constant and the isosteric heat of adsorption at low pressure. Building on those fundamental expressions, we then introduce a series expansion of a related thermodynamic quantity in (inverse) temperature space, which allows for temperature extrapolation of both the Henry’s law constant and isosteric heat of adsorption, using extrapolation coefficients that may be computed from the adsorbent-adsorbate potential energy by numerical or Monte Carlo integration. In Section 3, we present results that compare direct calculations of the Henry’s law constant and isosteric heat to extrapolations of the same, for both a simple system and more complicated adsorbents that are represented atomistically. Finally, we summarize the main findings of our work in Section 5 including a general recommendation for use of the extrapolation method, and discuss possible extensions of the method.

2 Theory and Methods

In the following section, we present the statistical mechanical expressions for the Henry’s law constant and isosteric heat of adsorption and the mathematical manipulations that yield

an extrapolation of those quantities in temperature. We also briefly describe the method for computing the extrapolation coefficients, which is just an extension of the existing technique for calculating the Henry’s law constant.

2.1 Henry’s Law for Adsorption

Definition of the Henry’s law constant for adsorption is straightforward and need not be presented in detail here. For an efficient presentation of the Henry’s law constant, we suggest the reader visit the discussion of Sarkisov from 2012.¹⁸ The derivation presented there, which is itself grounded in the previous work of June et al.,²⁸ is a clear and succinct starting point for our discussion. In those works, the Henry’s law constant $K_H(T)$ is defined via

$$K_H(T) = \lim_{p \rightarrow 0} \frac{N_{\text{ads}}(p, T)}{p} \quad (1)$$

i.e., that in the limit of low pressure, the amount of adsorbed gas per unit mass of adsorbent (N_{ads}) is proportional to the partial pressure of the adsorbate (p); the constant K_H is a function of temperature T . After constraining the system such that both the adsorbent and adsorbate are rigid, and incorporating statistical-mechanical expressions for N_{ads} and p , one can show that¹⁸

$$K_H(T) = \frac{1}{\rho_S k_B T} \langle \exp[-\beta U(\mathbf{r}, \psi)] \rangle \quad (2)$$

where k_B is the Boltzmann constant, $\beta = 1/k_B T$, and ρ_S is the bulk density of the adsorbent. $U(\mathbf{r}, \psi)$ is the potential energy interaction between a single adsorbate molecule and the adsorbent, when the adsorbate is at position \mathbf{r} and in orientation ψ . Here and throughout this work, the $\langle \dots \rangle$ brackets indicate a spatial-orientational average of the quantity in the brackets, and ρ_S appears as a normalization constant so that N_{ads} is given relative to the mass of adsorbent. Thus, stated simply, the Henry’s law constant is proportional to the average Boltzmann factor of the interaction energy of one adsorbate molecule with the adsorbent.

The isosteric heat of adsorption in the limit of zero pressure or infinite dilution of the

adsorbate is given by¹⁸

$$q_{\text{st}}^{\infty}(T) = \left(\frac{\partial \ln K_{\text{H}}}{\partial \beta} \right) = \frac{1}{\beta} - \frac{\langle U(\mathbf{r}, \psi) \exp[-\beta U(\mathbf{r}, \psi)] \rangle}{\langle \exp[-\beta U(\mathbf{r}, \psi)] \rangle} \quad (3)$$

Both the Henry's law constant and the low-pressure isosteric heat of adsorption are closely related to the single-molecule potential energy, through spatial-orientational averages of its Boltzmann factor and the first moment of that average. As we discuss in a subsequent section, both K_{H} and q_{st}^{∞} may be computed with a suitable integration strategy when $U(\mathbf{r}, \psi)$ is known.

2.2 Temperature Extrapolation

Let us now consider the temperature dependence of K_{H} . For ease of manipulation, we rewrite K_{H} as a function of the inverse temperature β and define a new intermediary function $K(\beta)$, such that

$$K_{\text{H}}(\beta) \equiv \frac{\beta}{\rho_{\text{S}}} K(\beta) \quad (4)$$

where

$$K(\beta) = \langle \exp[-\beta U(\mathbf{r}, \psi)] \rangle \quad (5)$$

Then, following previous work on temperature extrapolation,^{22-24,26} $K(\beta)$ may be expanded as an M^{th} -order Taylor series about a basis inverse temperature, $\beta = \beta_0$, as

$$\begin{aligned} K(\beta) &\approx K(\beta_0) + \sum_{j=1}^M \frac{1}{j!} \left(\frac{\partial^j K}{\partial \beta^j} \right) \Big|_{\beta_0} (\beta - \beta_0)^j \\ &\approx \sum_{j=0}^M K_j(\beta_0) (\beta - \beta_0)^j \end{aligned} \quad (6)$$

where the Taylor coefficients K_j are given by

$$K_j(\beta) = \frac{1}{j!} \left(\frac{\partial^j K}{\partial \beta^j} \right) = \frac{(-1)^j}{j!} \langle U(\mathbf{r}, \psi)^j \exp[-\beta U(\mathbf{r}, \psi)] \rangle. \quad (7)$$

The important result of this Taylor-series expansion of $K(\beta)$ is that the coefficients of the expansion are given by spatial-orientational averages of powers of the single-molecule potential energy multiplied by the Boltzmann factor of that same energy. These coefficients are ostensibly calculable given a model for $U(\mathbf{r}, \psi)$ for arbitrary j ; we only note that U is raised to the j power, which may eventually lead to floating-point limitations in computer-based calculations of K_j . Substituting eqs 6 and 7 into eq 3 and taking a derivative of $K(\beta)$ yields q_{st}^∞ as a series-based form involving the K_j coefficients:

$$q_{\text{st}}^\infty(\beta) = \frac{1}{\beta} + \frac{\sum_{j=1}^M j \cdot K_j(\beta_0) (\beta - \beta_0)^{j-1}}{\sum_{j=0}^M K_j(\beta_0) (\beta - \beta_0)^j} \quad (8)$$

We note that $q_{\text{st}}^\infty(\beta) = 1/\beta + K_1(\beta)/K_0(\beta)$; previous calculations of q_{st}^∞ were already utilizing what we define as K_1 . Alternatively, one may develop an extrapolation of q_{st}^∞ itself instead of reusing the extrapolation of $K(\beta)$; however, we found such a “direct” extrapolation of q_{st}^∞ to perform inconsistently in comparison to the extrapolation method in eq 8. We will revisit this point in the conclusions section of the present work.

The expansion of $K(\beta)$ in eq 6 theoretically allows for estimation of K_{H} and q_{st}^∞ via extrapolation after computation of the K_j coefficients. Given that many coefficients can be computed ($M \gg 1$), the extrapolation may be used to make accurate predictions at temperatures “far” from the basis temperature β_0 . Later sections of this work will demonstrate how far in temperature (more properly, β) space the extrapolation can be done reliably.

Before proceeding, we must briefly comment on the relationship between the extrapolation in eq 6 and the Clausius-Clapeyron expression in eq 3. If q_{st}^∞ is constant, then K_{H} may be analytically extrapolated to any temperature from a measurement of K_{H} at a single basis temperature. However, q_{st}^∞ is “rarely” not a function of temperature.²⁹ Thus, the second-order and higher derivatives of $K(\beta)$ can be alternatively thought of as corrections to q_{st}^∞ in the context of eq 3. The utility of the extrapolation of $K(\beta)$ stems from the fact that the

variation of q_{st}^∞ with temperature is too large for first-order extrapolation to be accurate for any nontrivial $\Delta\beta$.

2.3 Monte Carlo Integration

Calculation or estimation of K_{H} and q_{st}^∞ is possible given a force field or model for $U(\mathbf{r}, \psi)$. If $U(\mathbf{r}, \psi)$ can be represented by an analytic function (e.g., a smeared Lennard-Jones potential that is a function of a tractable set of spatial variables), then it is at least theoretically possible to directly compute K_{H} and q_{st}^∞ ; we later show an example where numerical integration is used to obtain K_j . In practice, and especially for multisite adsorptive molecules where the orientation vector ψ is non-negligible, it is more common to compute the relevant integrals numerically via MC integration, i.e., by the Widom insertion technique.³⁰ One can use the same technique to estimate the K_j expansion coefficients, e.g.,

$$\overline{K_j}(\beta) = \frac{(-1)^j}{j!} \frac{1}{N_{\text{mc}}} \sum_{l=1}^{N_{\text{mc}}} U(\mathbf{r}_l, \psi_l)^j \exp[-\beta U(\mathbf{r}_l, \psi_l)] \quad (9)$$

where (\mathbf{r}_l, ψ_l) is a random position and orientation of the adsorbate, and is generated N_{mc} times. Here, the overline indicates that the annotated quantity is an *unbiased estimator* of the true value; additionally, there is statistical uncertainty associated with $\overline{K_j}$ which can itself be estimated (cf. Section SI.II. of the Supporting Information [SI]). To streamline discussion, we will use an overhat to identify a quantity estimated by extrapolation, e.g.,

$$\widehat{K_{\text{H}}}(\beta) = \sum_{j=0}^M \overline{K_j}(\beta_0) (\beta - \beta_0)^j \quad (10)$$

and similarly for $\widehat{q_{\text{st}}^\infty}$. These extrapolant estimates have uncertainty from both the uncertainty in the expansion coefficients and the extrapolation of $K(\beta)$ itself, though in the present work we only consider uncertainty from the coefficients. Selection of a satisfactory N_{mc} depends heavily on the characteristics of the adsorption system (temperature, adsorbent,

and adsorptive). Larger N_{mc} , of course, reduces uncertainty in the integral, at the cost of longer run time. We will initially present results using fixed N_{mc} (order 10^6), but will later utilize an autotuning strategy to free the integration scheme from manual inputs.

3 Results and Discussion

In the following section, we present results that demonstrate extrapolation of K_{H} and q_{st}^{∞} for various adsorption systems. Key points to examine are the basis temperature (β_0), acceptable ranges of β for reliable interpolation, the extrapolation order (M value), and the relationship between integral convergence (i.e., uncertainty in the extrapolation coefficients) and extrapolation results. In all of the results that follow, we utilize models for $U(\mathbf{r}, \psi)$ disclosed in previous literature, and implement all but one set of MC calculations using the open-source FEASST toolkit.³¹ The isosteric heat for one system is additionally calculated using RASPA,³² simply to verify that FEASST and RASPA return the same results. A sample notebook that demonstrates the use of FEASST for these calculations is provided with the SI.

3.1 Demonstration: Direct Calculation for an Analytic Potential

As mentioned previously, both K_{H} and the K_j coefficients can be computed directly when $U(\mathbf{r}, \psi)$ is available in analytic form. While it is essentially effortless in this case to compute K_{H} at any temperature, comparing the direct calculation of K_{H} to an extrapolated estimate serves to demonstrate the predictive ability of the extrapolation and identify limitations to it. Additionally, the comparison can be done without concern for convergence of MC integrals.

For a demonstration system, we examined the adsorption of argon in a multiwall carbon nanotube (MWCNT), where the Ar/MWCNT $U(\mathbf{r}, \psi)$ is modeled using the Cylindrical Steele 10-4-3 Potential.³³ Parameters used for the Lennard-Jones Ar and carbon were identical to those used in our previous study of the system by MC simulation,³⁴ and, for this

demonstration, the radius of the MWCNT was $R = 3.405$ nm (10 times the σ parameter of argon). To reduce ambiguity, we based the Henry’s law constant on adsorption *per unit length of MWCNT*, i.e., the normalizing “density” ρ_S in eq 2 is the length-to-volume ratio of the MWCNT, $1/(\pi R^2)$. Finally, we computed both K_H and K_j for $M = 20$ using conventional numerical integration.

Figure 1 shows both the directly calculated $K_H(T)$ and extrapolated $\widehat{K}_H(T)$ for the Ar/MWCNT system. Because $U(\mathbf{r}, \psi)$ is analytic, the K_j coefficients may be computed by numerical integration. We checked the numerical integration to confirm that the results were not dependent on the numerical grid; thus the resultant K_j are essentially exact. Thus, any differences between $K_H(T)$ and $\widehat{K}_H(T)$ may be attributed to extrapolation alone. For the 20th-order extrapolation, there is remarkable agreement for all four extrapolation estimates of $\widehat{K}_H(T)$, except at low temperature (say, below 50 K) and at high temperature for the extrapolation from $T_0 = 100$ K, though we urge some caution in interpretation since the y-axis is plotted on a logarithmic scale. For example, at $T = 50$ K, the extrapolation from $T_0 = 100$ K underpredicts K_H by 0.73 %, where as that from $T_0 = 400$ K underpredicts K_H by 42 %. At 350 K, the underprediction of K_H is less than 0.0002 %, except for that from $T_0 = 100$ K which is visibly overpredicted by three orders of magnitude. At 200 K, the $T_0 = 100$ K extrapolation overpredicts K_H by 2.3 %, and extrapolations from the other bases are effectively exact, with less than 10^{-7} % deviation from the true value. In Figure 2, corresponding results are shown for the isosteric heat of adsorption. As for K_H , extrapolation of q_{st}^∞ is very accurate for the three largest basis temperatures, while also failing at low T . Remarkably, however, the extrapolations from higher T_0 are accurate down to nearly 100 K, while also reproducing q_{st}^∞ up to 600 K. Deviation from the actual q_{st}^∞ is essentially undetectable on the same range, with calculated maximum deviation of 0.02 % (neglecting the results for $T_0 = 100$ K). Over this temperature range, the extrapolations using the three highest basis temperatures also capture two nontrivial extrema.

The results in Figures 1 and 2 draw out themes that will also be seen in subsequent

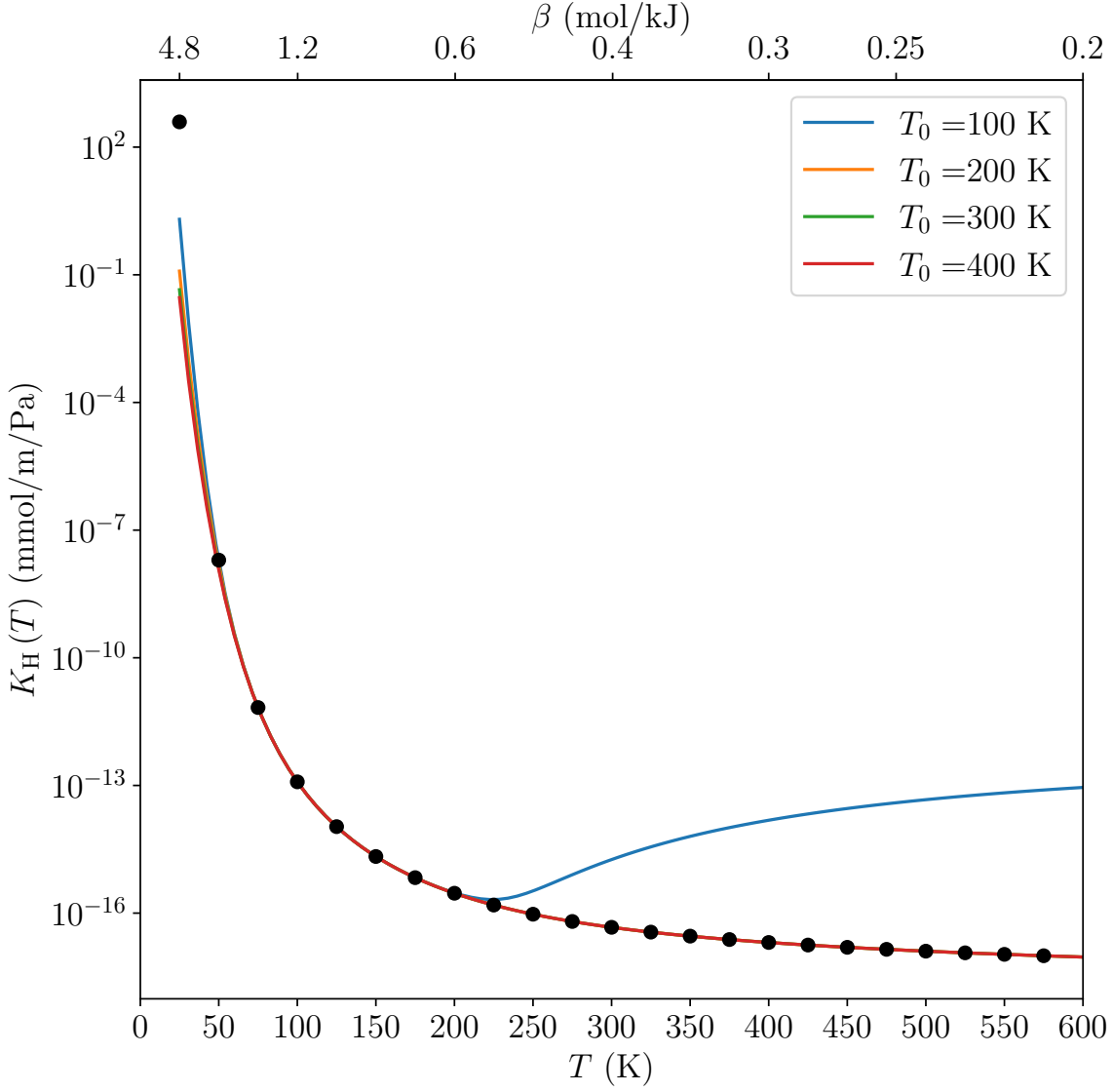


Figure 1: Henry Law Constant for the Ar/MWCNT system described in the text. Directly-measured K_H are shown by the black points and 20th-order extrapolations are shown by solid lines; line color identifies the basis temperature (T_0) of the extrapolation. The secondary horizontal axis shows $\beta = 1/k_B T$ equivalent to the linear temperature scale on the primary axis.

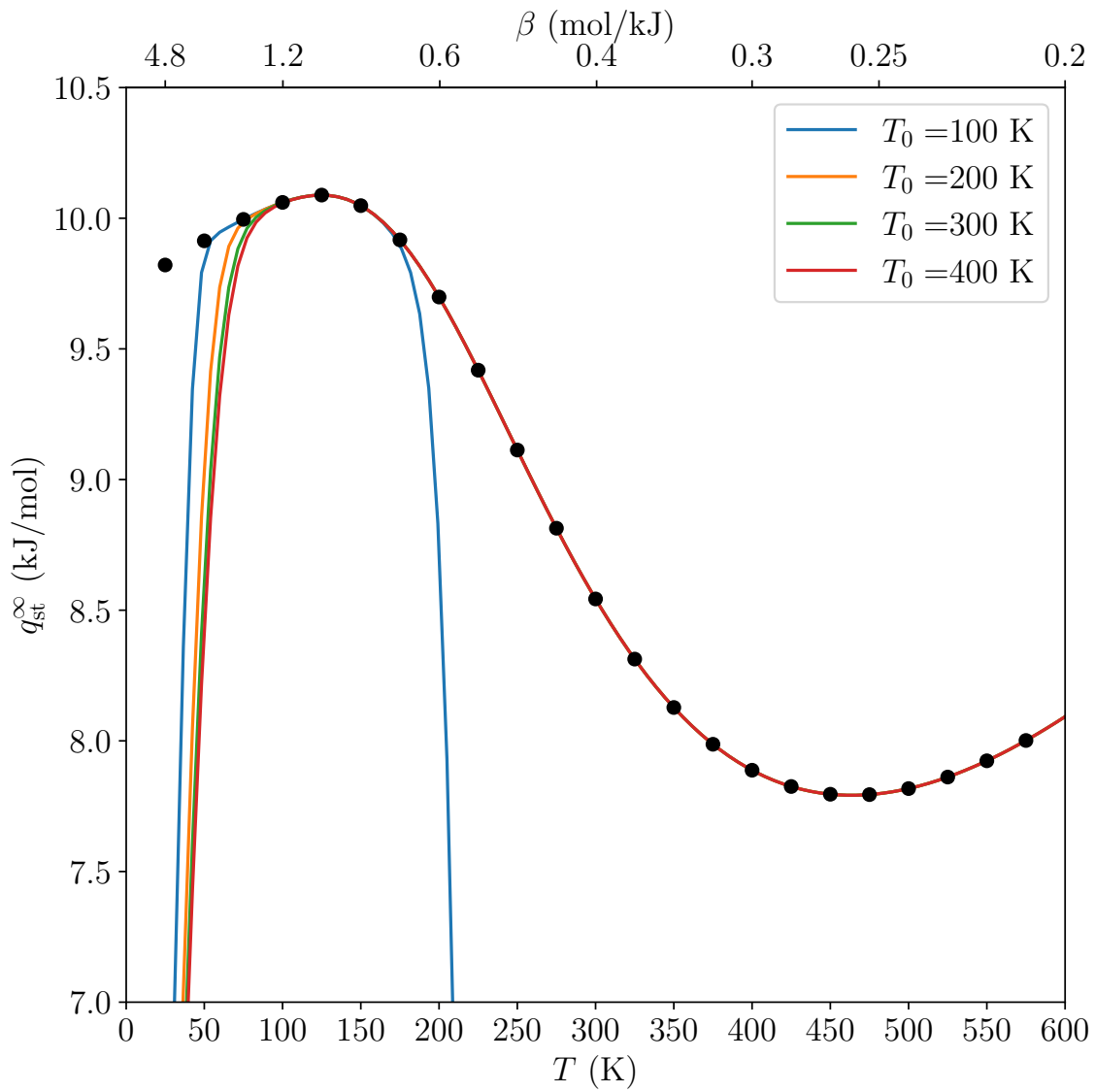


Figure 2: As Figure1, for the isosteric heat of adsorption q_{st}^{∞} .

examples. First, extrapolations typically fail at very low temperature regardless of the basis temperature, which is essentially identical to results for previous temperature extrapolations of phase equilibrium conditions²² and virial coefficients.²⁶ Second, extrapolation of K_H and q_{st}^∞ can be quite reliable and reproducible regardless of T_0 over a nontrivial range of temperature. This range is better defined in terms of distance in β space, which appears naturally as $(\beta - \beta_0)$ in the Taylor-series-based expressions eqs 6 and 8. To demonstrate this, Figures 1 and 2 include the β scale as a secondary horizontal axis. The temperature range $50 \text{ K} < T < 600 \text{ K}$ is a range of 2.2 mol/kJ in β space, a range where the extrapolations of K_H are remarkably consistent for the higher- T_0 extrapolations. In comparison, the range from 25 K to 50 K is actually a larger β range of 2.4 mol/kJ. For q_{st}^∞ , the extrapolations are consistent from 100 K to 600 K, a range of 1 mol/kJ in β space. The combination of these two observations yields a general strategy for extrapolating K_H and q_{st}^∞ : generate the extrapolation coefficients at “high” T_0 , but extrapolate within a “small” range of β around β_0 . Thus, it is desirable to choose T_0 near the midpoint of the range of desired β . Based on Figures 1 and 2, an extrapolation range of *at most* $|\beta - \beta_0| < 0.5 \text{ mol/kJ}$ is safe, for all of the extrapolations shown. We qualify this suggestion with “at most” because of mathematical limitations: $\Delta\beta = +0.5 \text{ mol/kJ}$ leads to a realistic suggestion for the minimum T , whereas $\Delta\beta = -0.5 \text{ mol/kJ}$ may result in a negative β depending on the basis β_0 . Thus, the lower β extrapolation limit must be selected using some caution. A final caveat is that extrapolation of q_{st}^∞ cannot extend to as low a temperature as K_H .

3.2 Example: CO₂ Adsorption in ZIF-8

We continue with an examination of the Henry’s law properties of CO₂ in the MOF ZIF-8, a system that has been simulated frequently.^{34–36} We modeled CO₂ using the TraPPE potential³⁷ and the ZIF-8 MOF using the force field introduced by Zhang and Snurr,³⁸ with cross-site interactions set via Lorentz-Berthelot combining rules. Partial charges were handled via the Ewald summation technique, with Ewald parameters set via the recipe from

DLPOLY³⁹ with a relative tolerance of 10^{-5} . Pair energies were truncated at 12 Å, with linear force-shift corrections to the Lennard-Jones terms. We estimated \widehat{K}_H and the \overline{K}_j coefficients with $M = 20$, using $N_{\text{mc}} = 10^6$, at $T_0 = 250$ K, 350 K, 450 K, and 550 K.

Figure 3 shows the direct calculations of K_H for this system, as well as extrapolation estimates \widehat{K}_H for $150 \text{ K} < T < 650 \text{ K}$ using coefficients estimated at the four basis temperatures. The main result demonstrated in Figure 3 is that the extrapolation method provided here is able to accurately reproduce K_H for $T > 250$ K using any of the four basis temperatures. Furthermore, the extrapolation is remarkably consistent down to 150 K for all coefficient sets save that of the highest basis temperature 550 K. At the four temperatures where K_H was calculated directly, the extrapolations all predict \widehat{K}_H within 0.3 % of the directly calculated K_H , except for the extrapolation from 550 K to 250 K, where the deviation is only 1 %. These results are qualitatively consistent with those for the analytic potential in Section 3.1: Extrapolations are consistent provided that the basis temperature is high and the extrapolation range in β space is relatively small. In this case, extrapolation using a basis temperature of $T_0 = 550$ K becomes unreliable when $\beta - \beta_0 > 0.5$ mol/kJ. This yields a similar recommendation as for the Ar/MWCNT system: a safe suggestion for the lower extrapolation T is based on a maximum of $\Delta\beta = 0.5$ mol/kJ.

Figure 3 also displays uncertainty estimates for $\widehat{K}_H(T)$ for $T_0 = 350$ K and $M = 10$, as computed by the method described in the SI. In the figure, the error bars are only visible for $T \leq 200$ K, furthest in terms of β from the basis β_0 . The uncertainty is low, 8 % at $T = 150$ K and decreasing to 0.6 % at 650 K. As expected, the uncertainty generally increases with distance from the basis temperature in β space. (For reference, uncertainty in the direct calculations of K_H is below 0.4 %.) In this particular case, the low uncertainty in \widehat{K}_H is reflective of low uncertainty (good convergence) in the measured \overline{K}_j : ranging from 1 % for $j = 0$ to 19 % for $j = 20$.

Figure 4 displays the isosteric heat of adsorption for the same CO₂/ZIF-8 system determined via direct calculation and extrapolation. In general, the previous observations for

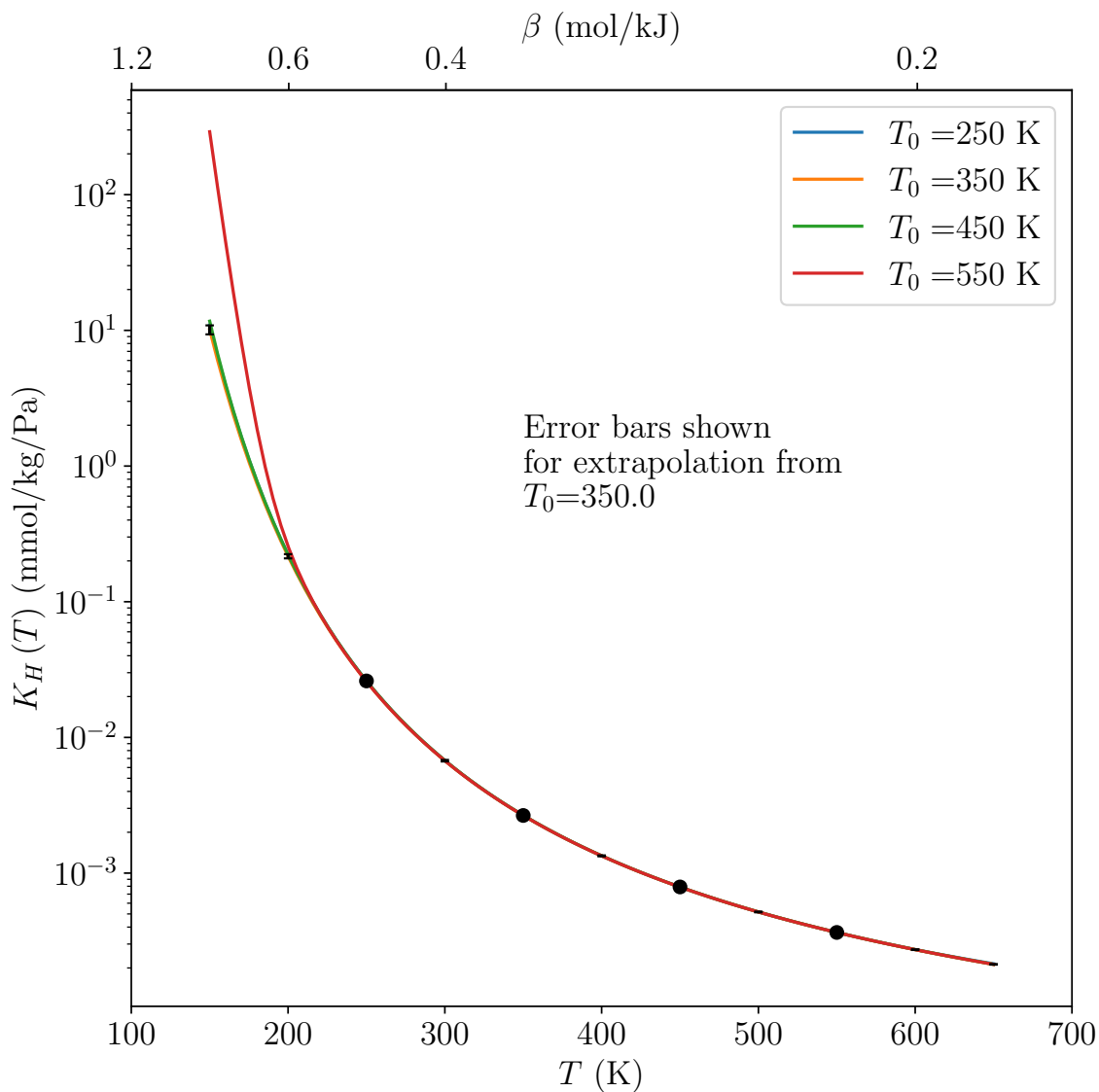


Figure 3: Henry’s law constant for a CO₂/ZIF-8 system, computed by MC integration and by temperature extrapolation, using the model described in Section 3.2. Directly-measured K_H are shown by the black points, while estimates by extrapolation are shown by solid lines; line color identifies the basis temperature (T_0) of the extrapolation. Uncertainty estimates, based on statistical uncertainty in \overline{K}_j , are shown for the extrapolation from $T_0 = 350$ K, as black error bars at select temperatures. Uncertainty estimates on direct measurements of K_H were smaller than 0.4 % and are consequently not visible.

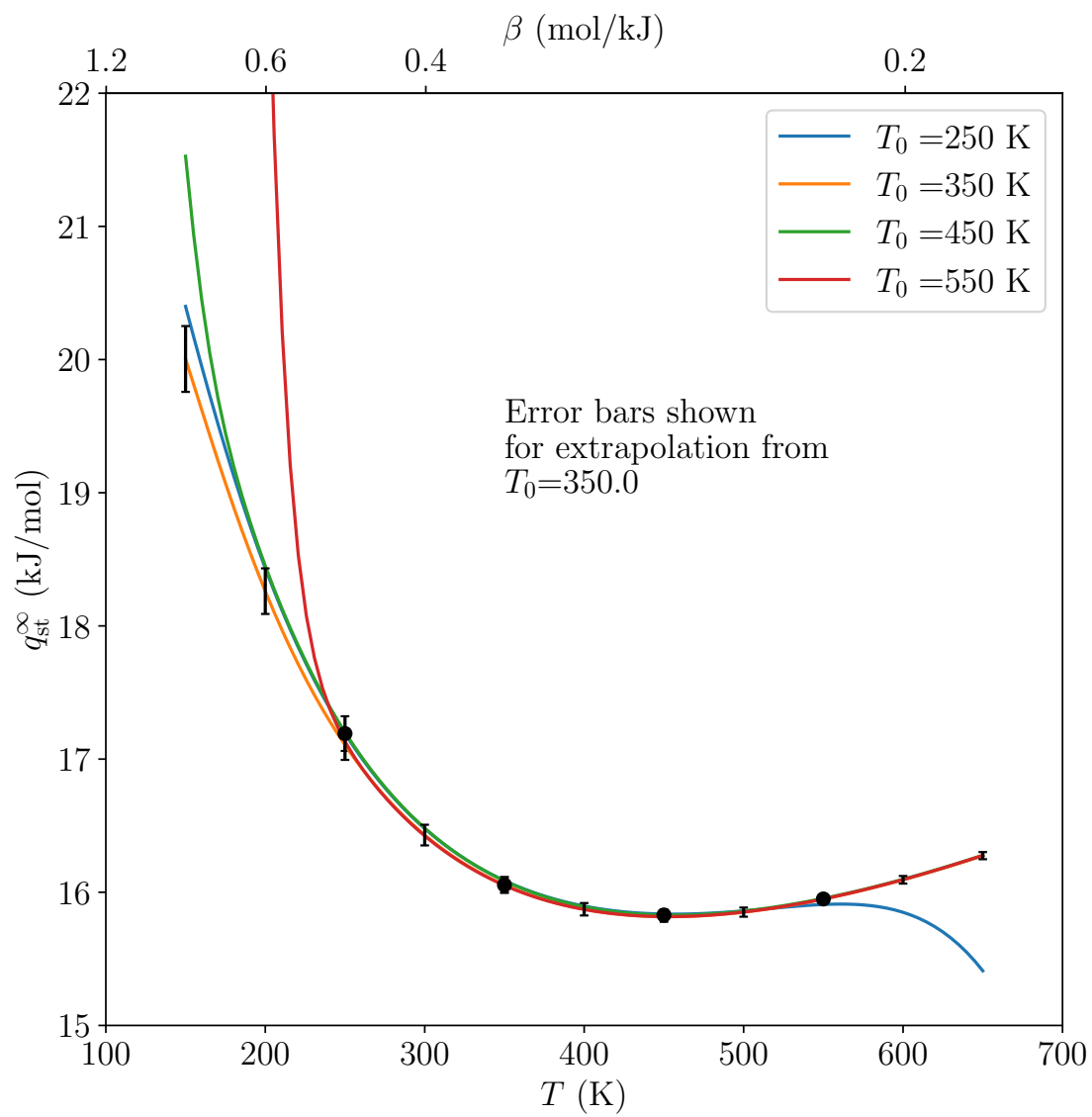


Figure 4: As Figure 3, for the isosteric heat of adsorption q_{st}^{∞} .

the Henry’s law constant hold for the isosteric heat of adsorption: $\widehat{q_{\text{st}}^\infty}$ from the four basis temperatures agree well with direct calculations of q_{st}^∞ and are relatively consistent for $250 \text{ K} < T < 550 \text{ K}$. At the four temperatures where q_{st}^∞ was calculated directly, the extrapolations deviate from the direct calculation by 0.3 % at most. The extrapolation from $T_0 = 550 \text{ K}$ deviates earlier than that for K_{H} by approximately 100 K. Both of these observations follow from the fact that the heat of adsorption depends on both $K(\beta)$ and its first derivative. The uncertainty in an extrapolation of q_{st}^∞ from $T_0 = 350 \text{ K}$ is actually lower than that for K_{H} , ranging from 1.2 % at 150 K to 0.2 % at 650 K. The general rule of thumb suggested by previous results holds for q_{st}^∞ : Extrapolation can be done reliably and accurately provided that T_0 is large and the extrapolation range in β is small. The only caveat added by the q_{st}^∞ results is that the range of acceptable extrapolation in β is smaller for q_{st}^∞ than K_{H} ; Figure 4 suggests a lower T based on $\Delta\beta = +0.35 \text{ mol/kJ}$.

Figure 5 shows $\widehat{K_{\text{H}}}$ for the $\text{CO}_2/\text{ZIF-8}$ system from $T_0 = 350 \text{ K}$, using different numbers of coefficients (M values). As expected, lower-order extrapolations far from T_0 perform poorly compared to higher-order extrapolations. In particular, order $M \geq 10$ are nearly indistinguishable within the scale of Figure 5, except for the lowest temperature extrapolations where the distance in β -space is relatively large. At 150 K, for example, the $M = 20$ extrapolation is 36 % larger than that for $M = 10$.

Although higher-order extrapolations may be more accurate at temperatures far from T_0 , the uncertainty at those temperatures can increase with M . (Error bars for $M = 10$ are shown as an example in Figure 5, but are barely visible.) For $T > 250 \text{ K}$, uncertainty in the extrapolation is essentially unchanging for $M > 10$ (data are not shown in the figure); at 150 K, however, the uncertainty in $\widehat{K_{\text{H}}}$ increases nearly from 0.104 mmol/kg/Pa for $M = 10$ to 0.177 mmol/kg/Pa for $M = 20$, a nearly 70 % increase. This is reflective of uncertainty in $\overline{K_j}$: $\overline{K_0}$ (350 K) converged to 1 % relative uncertainty, $\overline{K_{10}}$ (350 K) converged to 9 %, and $\overline{K_{20}}$ (350 K) converged to only 19 %. (For comparison, the same coefficients at 450 K converged to 0.7 %, 8 %, and 1.5 % relative uncertainty.) These results suggest that the sta-

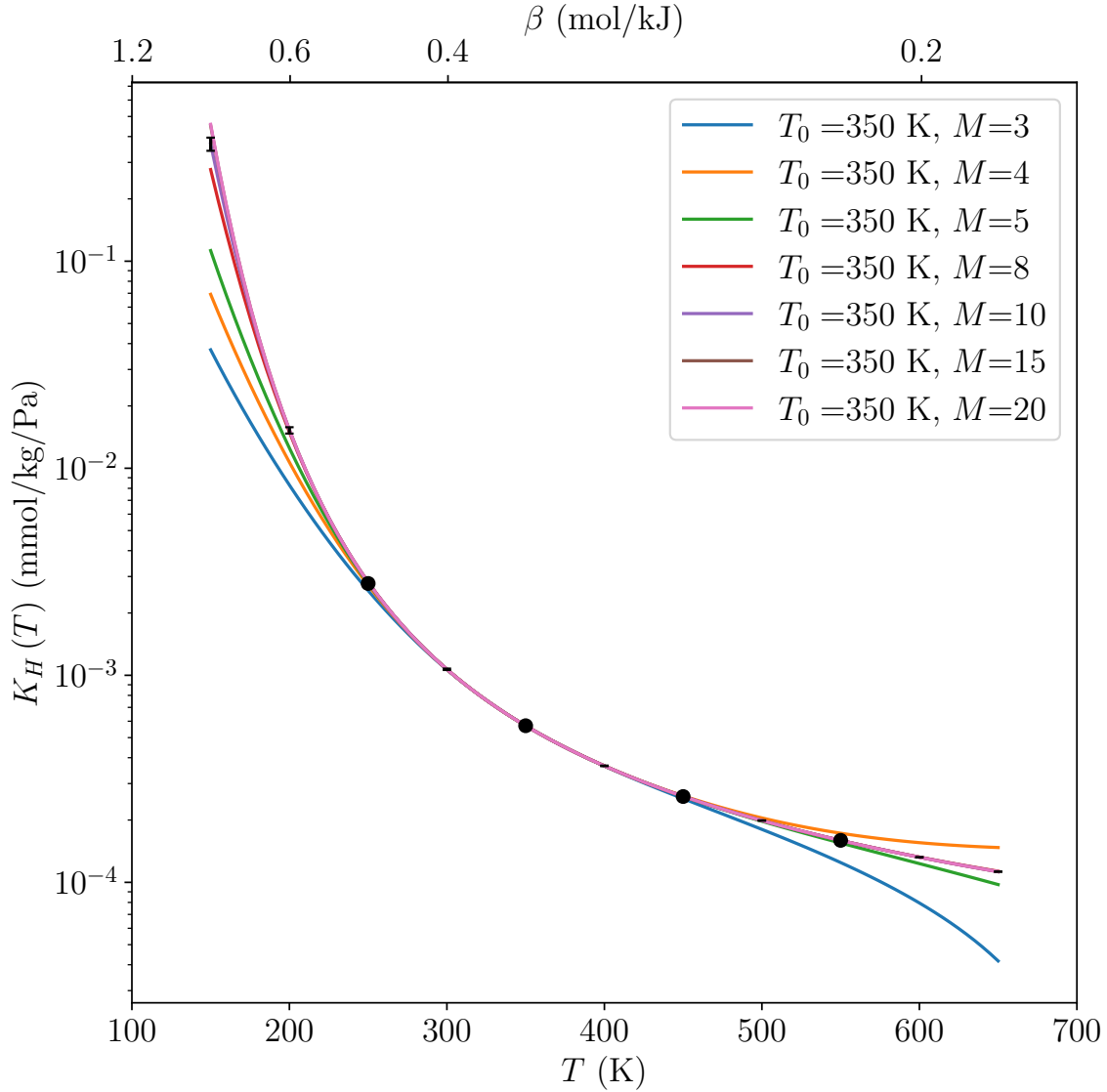


Figure 5: Henry's law constant for the $\text{CO}_2/\text{ZIF-8}$ system, computed directly and by extrapolation. The solid points are the same direct measurements of K_H in Figure 3. The solid lines are \widehat{K}_H extrapolations from $T_0 = 350$ K, with different numbers of series coefficients (M values). Error bars are the statistical uncertainty of the extrapolation with $M = 10$.

tistical uncertainty in an extrapolation of K_H should be scrutinized carefully; increasing M may incur increasing uncertainty that is numerically unacceptable. Increasing M does come at some computational cost; the calculation of K_j for the CO₂/ZIF-8 system with $M = 20$ took 30 % more time than that for $M = 10$. (We urge caution in interpreting this statistic: the nonlinear scaling of the calculation time reflects the fact that a single calculation of $U(\mathbf{r}, \psi)$ is used to update the running averages of all K_j . For the Ar/MWCNT system discussed earlier, which has a simpler $U(\mathbf{r}, \psi)$, increasing M from 10 to 20 increases calculation time by 40 %.) Alternatively, uncertainty in $\overline{K_j}$ may be reduced by increasing N_{mc} , which ultimately reduces uncertainty in the extrapolated $\widehat{K_H}$, though at increased computational cost. Thus, the optimal choice of M depends on a variety of concerns: the number of MC trials, the acceptable level of uncertainty, and what is an appropriate computation time.

3.3 Other Examples for MOFs and Zeolites

Section S1.1 of the SI includes results for other example systems where the adsorptive is a small molecule and the adsorbent is represented atomistically: an all-silica form of FAU zeolite with N₂ and H₂O, ZIF-8 with H₂O, and IRMOF-1 with CO₂. The results for those cases are qualitatively identical to the results for the CO₂/ZIF-8 system in that extrapolation of K_H is quite successful for a high T_0 provided that $|\beta - \beta_0|$ is small. Similarly, extrapolation of q_{st}^∞ is similarly successful, but cannot extend to as low a temperature as the extrapolation of K_H . As for the CO₂/ZIF-8 system, maximum extrapolation ranges of $|\beta - \beta_0| < 0.5$ mol/kJ for K_H and $|\beta - \beta_0| < 0.35$ mol/kJ for q_{st}^∞ are suggested by those results. We note that calculations with H₂O in ZIF-8 required higher N_{mc} than the case with CO₂ to yield a satisfactory extrapolation.

3.4 Large Scale Screening Application: CoREMOF-2019

As discussed in the Introduction, K_H is frequently used as an adsorption characteristic for screening materials, especially as a first-pass discriminator due to its ease of calculation.

To demonstrate how the temperature extrapolation of K_H can be introduced into a screening scheme, we apply it to a mass set of adsorbents, the metal-organic frameworks in the CoREMOF-2019 set¹³ (11 660 materials in total). We mimicked a minimal-input screening exercise by using a common simulation setup and forcefield for all materials: Atoms in the MOFs were modeled as LJ sites with parameters set by the Universal Force Field⁴⁰ and with partial charges set by the m-CBAC method.⁴¹ The MOF unit cell was replicated in all directions to allow use of a 12 Å cutoff radius. Energies were calculated with the same techniques and parameters used for the CO₂/ZIF-8 system. To improve convergence of the MC integrals, we added an auto-termination scheme to the calculation. First, the MC integrations for $\overline{K_j}$ used at least 10^6 and no more than 5×10^7 trial insertions. Second, the calculation terminated early if $\overline{K_0}$ converged to less than 1 % uncertainty and $\overline{K_{10}}$ converged to less than 5 % uncertainty. These convergence criteria were selected subjectively to balance runtime with acceptable uncertainty. As we will point out shortly, many systems used the full 5×10^7 trials without converging to the desired uncertainty.

Figure 6 compares the directly-measured K_H with $\widehat{K_H}$ from either $T_0 = 450$ K or 600 K, with $M = 20$, for the materials in the CoREMOF-2019 set. The plot has been truncated at a very high value of $K_H = 10^5$ mmol/kg/Pa, to enable easier identification of deviations from experimentally reasonable values of K_H . (For reference, at 450 K, only 1270 materials have $K_H > 10^{-1}$ mmol/kg/Pa, and 340 materials have $K_H > 10$ mmol/kg/Pa.) The primary result is that extrapolation of K_H from $T_0 = 600$ K down to 450 K (blue points) is outstanding when compared with the direct measurements at 450 K. Deviation between the direct calculation at 450 K and the extrapolation from 600 K exceeds 10 % for only 121 materials in CoREMOF-2019. Additionally, only 29 of these 121 materials have $K_H(450 \text{ K}) < 10^{-1}$ mmol/kg/Pa. Cases where the extrapolation fails are predominantly those materials with extremely high Henry’s law constants at the select temperature of 450 K. The data set comparing direct measurements at 600 K to extrapolations from 450 K shows a similar situation, up to a limit: The extrapolation generally reproduces the directly calculated K_H up to 10^{-1} mmol/kg/Pa,

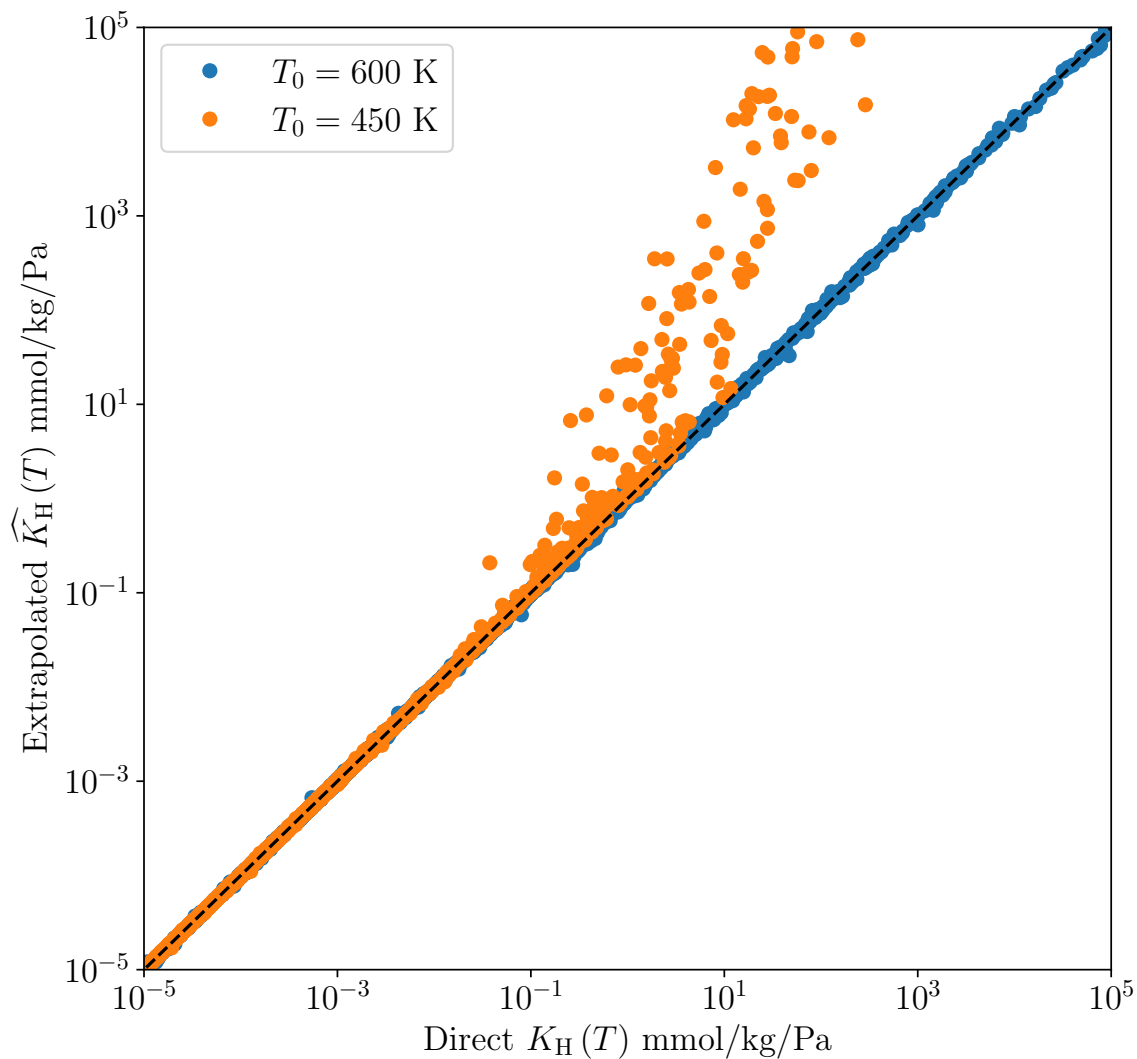


Figure 6: Comparison of direct MC estimates of K_H at 450 K and 600 K with extrapolations from $T_0 = 450$ K and 600 K, for the materials in the CoREMOF-2019 set, with $K_H < 10^5$ mmol/kg/Pa. The dashed line shows the $x = y$ diagonal. For visual clarity, uncertainty estimates are not shown.

after which a number of extrapolated points deviate significantly from the direct measurements of K_{H} , even by several orders of magnitude. Fortunately, however, the number of poor extrapolations is limited in scope: Only 220 materials show deviation that exceeds 10 %; of those materials, only 30 have $K_{\text{H}}(600 \text{ K}) < 10^{-1} \text{ mmol/kg/Pa}$. The vast majority of points are concentrated along the desired diagonal, below $K_{\text{H}}(600 \text{ K}) < 10^{-1} \text{ mmol/kg/Pa}$. While a larger number of extrapolations from $T_0 = 450 \text{ K}$ deviate from direct calculations than those from 600 K, the extrapolation from 450 K is still remarkably successful.

Figure 7 displays a comparison of the direct measurements at 450 K and 600 K with extrapolations from the same two temperatures for four materials where the extrapolation from 450 K overpredicted $K_{\text{H}}(600 \text{ K})$ by at least a factor of 10^3 . For all four materials in the figure, and for all other deviating cases that we examined manually, the extrapolations from 450 K show a positive slope with respect to T at some $T > 450 \text{ K}$, contrary to the expected trend where K_{H} continuously decreases with T (which is implied by a positive q_{st}^{∞} , see eq 3). The same violation (positive slope) is seen for the extrapolations from 600 K, so the same qualitative deviation we see for the extrapolation from 450 K to 600 K would eventually appear for those extrapolations as well. On closer examination, there is another concern for these cases where the extrapolation from low temperature to high temperature is poor: All of these materials failed to converge according to the desired autoconvergence criteria. In fact, for *every material* where the extrapolation to 600 K exceeded the direct measurement by more than 10 %, the MC integration used 5×10^7 trial insertions, but failed to converge according to the desired criteria. For the ZOMKAP and ELEROD materials, $\overline{K}_0(450 \text{ K})$ converged to only relative uncertainties of 9 % and 10 %, respectively. Not all materials failed to converge so dramatically: For LENGES, $\overline{K}_0(450 \text{ K})$ and $\overline{K}_{20}(450 \text{ K})$ converged to 1.4 % and 2.3 %, respectively, with 5×10^7 trial insertions. Thus, while poor convergence of the extrapolation coefficients (at least according to our subjective criteria) is a good indicator that an extrapolation may not accurately extend far from the basis T_0 , even some cases that appear to have well-converged \overline{K}_j may not extrapolate K_{H} reliably when K_{H} is extremely

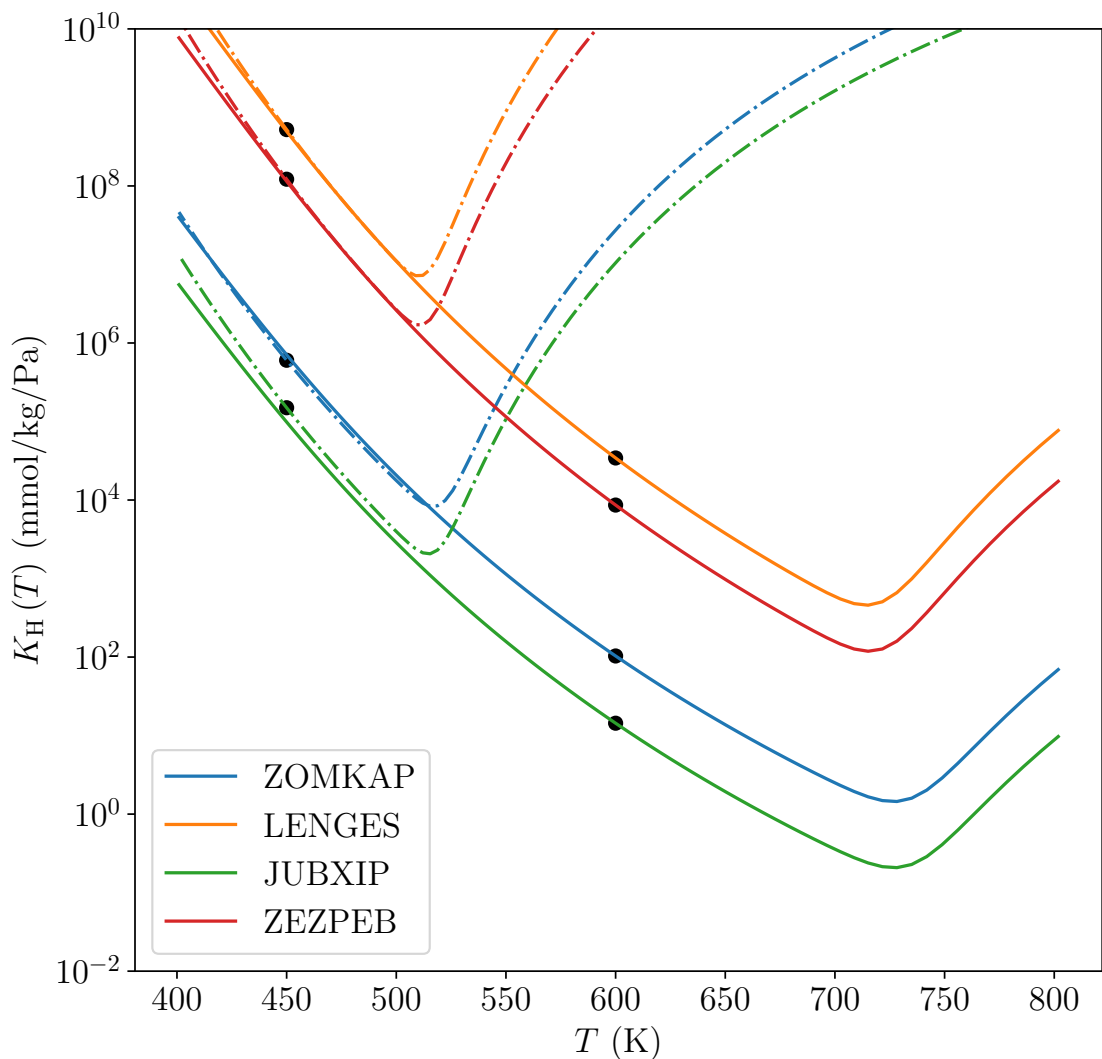


Figure 7: Plots of the direct and extrapolated K_H for four select materials from CoREMOF-2019, where the extrapolation estimate of $\widehat{K}_H(600 \text{ K})$ exceeds the directly estimated $K_H(600 \text{ K})$ by at least a factor of 10^{-3} . Black points are the direct estimates of K_H . Solid lines are the extrapolations from $T_0 = 600 \text{ K}$ and dashed-dot lines are the extrapolations from $T_0 = 450 \text{ K}$; line colors correspond to the material, as identified by a reference code in the figure legend.

large. As a final point of consideration, we tested the extrapolation of these problematic cases with $M < 20$ and found no general improvement versus the 20th-order extrapolation.

3.5 Strenuous Test: CO₂ Adsorption in ITQ-29

As a final demonstration of the temperature extrapolation of low-pressure adsorption properties, we examine the extrapolation of the isosteric heat for adsorption of CO₂ in a zeolitic material. This particular adsorption system was recently examined by Hyla et al.,⁴² who used molecular simulations to demonstrate a rare “significant temperature dependence” of the isosteric heat of adsorption: a decrease of approximately 12 kJ/mol in q_{st}^∞ between low and high temperatures. The results were confirmed by experimental measurements in the same paper. We revisited the system using the temperature extrapolation approach to investigate such behavior and test the extrapolation in what one may consider strenuous conditions.

The adsorbent material is an all-silica form of LTA zeolite, ITQ-29^{43,44} and the adsorbate is CO₂, where the system’s energy is modeled by a first-principles forcefield termed CCFF.⁴⁵ (Importantly, the sodalite cages of ITQ-29 were blocked as those regions are considered inaccessible to CO₂.⁴⁶) CO₂ is represented as a rigid molecule and the cross-interaction terms are given explicitly by the CCFF. (Strictly speaking, Ref 42 used the EPM2 model of CO₂,⁴⁷ without O-C-O bond deformation, but this is irrelevant for Widom insertion as adsorbate-adsorbate energy terms are not needed and the adsorbate is rigid.) Partial charges were handled identical to our previous simulations, though with Ewald parameters set with a relative tolerance of 10^{-6} (identical to Ref 42). Pair energies were cut at 11 Å (i.e., no tail correction or adjustment). To generate high-quality data, we computed $\overline{K_j}$ using 5×10^6 trial insertions with $M = 20$ at a number of temperatures between 10 K and 600 K, using FEASST, and then calculated $\widehat{q_{\text{st}}^\infty}$ directly and via extrapolation. For reasons explained shortly, we also computed q_{st}^∞ at select temperatures using RASPA.³²

Figure 8 plots $\widehat{q_{\text{st}}^\infty}$ from both the MC integration of Hyla et al. and our own simulations and

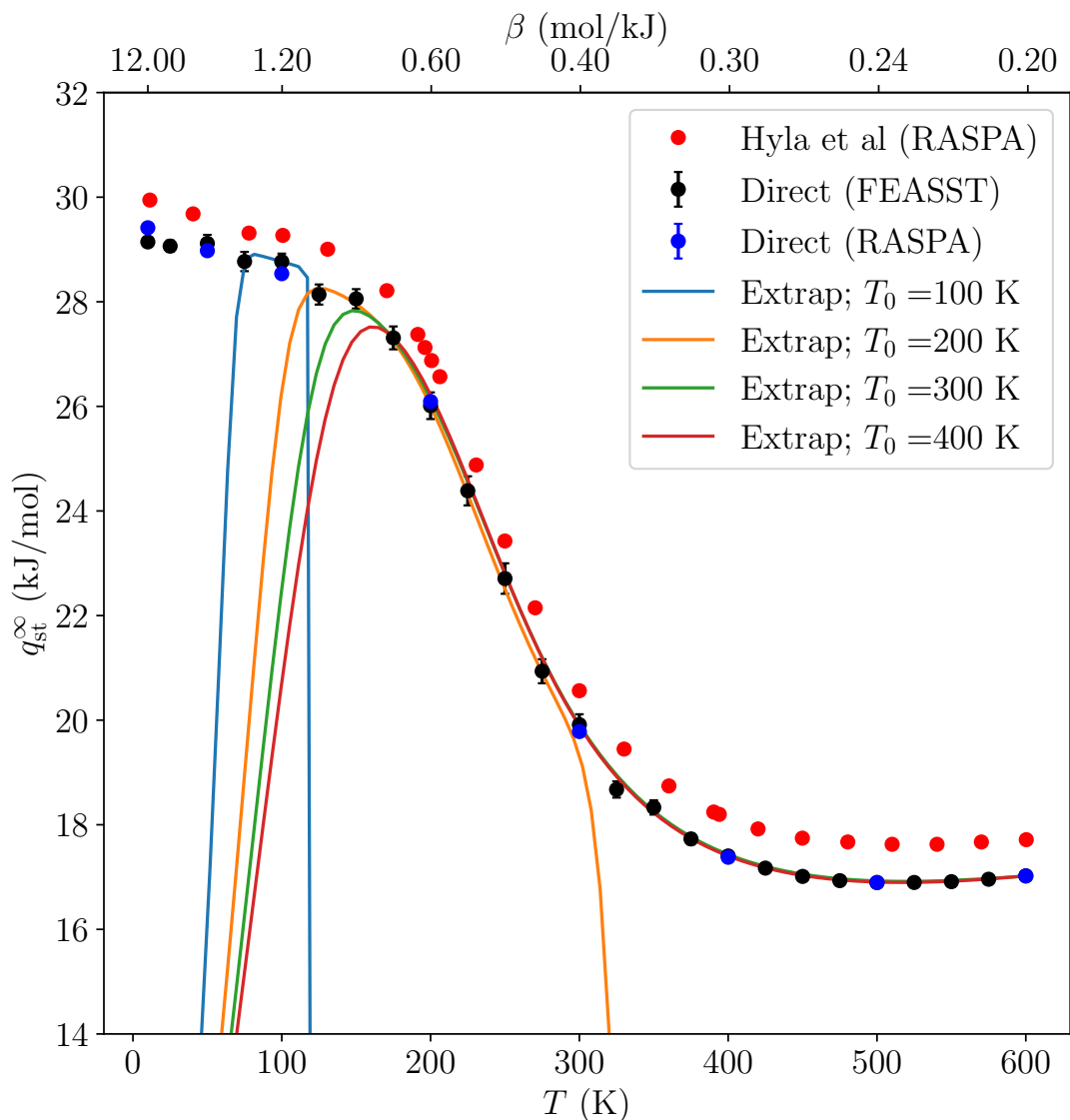


Figure 8: Isosteric heat of adsorption for CO_2 in ITQ-29. Solid points are direct measurements of K_H from MC integration by Hyla et al.⁴² (Figure 4 therein) and by the present authors using two MC toolkits. Error bars identify the 95 % confidence intervals for our direct measurements of K_H . Extrapolations are shown by solid lines, with the basis T_0 shown in the legend. The direct measurements from Hyla et al. have not been shifted. As mentioned in the text, we suspect that our implementation of the $\text{CO}_2/\text{ITQ-29}$ system differs slightly from that of Hyla et al.

calculations. The primary feature of interest is the large decrease in q_{st}^∞ over the temperature range shown: at low T the isosteric heat is about 29 kJ/mol, but then decreases to about 17 kJ/mol between 150 K and 400 K. Our MC integration results for q_{st}^∞ using FEASST reproduce the same trend as Hyla et al., but consistently lower by 0.5 kJ/mol to 0.8 kJ/mol, which was larger than the statistical uncertainty. For verification purposes, we re-ran the calculation using RASPA and reproduced the same q_{st}^∞ as FEASST, suggesting that our implementation of the CCFF for CO₂/ITQ-29 is probably slightly different than Hyla et al., and thus the apparent offset is not an issue of concern here.

The salient result is that the temperature extrapolation of q_{st}^∞ (with coefficients estimated in FEASST) can reproduce the temperature dependence of the directly calculated q_{st}^∞ , down to a temperature of about 175 K for bases $T_0 = 300$ K and 400 K. In all cases, the extrapolation fails at low temperature. We note that the extrapolation from $T_0 = 200$ K, while predictive to 150 K fails at $T > 300$ K. For $T_0 = 100$ K, the extrapolation is only predictive for ± 15 K. The results for this system are consistent with those for the MOF systems examined in detail: \overline{K}_j coefficients estimated at high-temperature yield good extrapolations, but fail at low temperature. Overall, the temperature extrapolation of q_{st}^∞ is outstanding and able to produce the full temperature dependence for $T > 175$ K.

We note that the extrapolations capture a nontrivial characteristic of the CO₂/ITQ-29 system. Hyla et al. attributed the significant temperature dependence of q_{st}^∞ to the spatial distribution of CO₂ in the zeolite at different temperatures. Specifically, CO₂ primarily resides in high-energy apertures at low temperature, while it instead samples the entire accessible pore structure at high temperature.⁴² Given the Boltzmann factor dependence in K_1 and K_0 (cf. eq 3), the contribution of the aperture energies to those terms carries more weight at low T , mathematically yielding a substantially larger q_{st}^∞ at low temperature than at high temperature. The extrapolation here is capturing the same temperature dependence even though the K_j extrapolation coefficients are based on the Boltzmann factor of $U(\mathbf{r}, \psi)$ at a single T_0 . This is more remarkable since, for our calculations, T_0 is 100 K to 200 K

higher than the temperature where CO₂ preferentially samples the apertures. That the extrapolation is still successful when the energy distribution of the adsorbate shifts to lower $U(\mathbf{r}, \psi)$ is a rather interesting effect that warrants further work, both for the CO₂/ITQ-29 system as well as other systems that exhibit nontrivial energy probability distribution (e.g., multiple adsorption sites).

4 Alternate Extrapolation Forms

For the present work, we have only presented the extrapolation in its simplest form: a Taylor series expansion of $K(\beta)$ which serves as a generating function for K_{H} and q_{st}^{∞} . Other extrapolation strategies are available and will be addressed in future work. First, one could use the K_j expansion coefficients to generate a Padé approximant of $K(\beta)$. We have explored Padé approximants for the systems examined in this manuscript and the SI and found that use of a Padé approximant can improve the predictive ability of the extrapolation. (See Figures SI.11 and SI.12 in the SI.) However, we had to manually tune the order of the approximant (e.g., the distribution of coefficients between the numerator and denominator polynomials) to retain numerical stability; some choices for the denominator order led to singularities in the resultant extrapolation. Additionally, we did not find that a particular Padé order was effective for all materials or adsorbates that we examined. Thus, we do not recommend use of a Padé approximant for extrapolating K_{H} or q_{st}^{∞} , as such approximants require human intervention to be stable and accurate. Second, an alternative approach for predicting K_{H} and q_{st}^{∞} involves construction of an interpolating polynomial between two basis temperatures.²⁷ In doing so, the combined extrapolation and interpolation may yield a prediction of K_{H} or q_{st}^{∞} that extends the predictive range further than the remarkable range shown here. We note, however, that this approach would require generation of a Taylor series for q_{st}^{∞} itself, as opposed to eq 8 which is actually generating q_{st}^{∞} through strategic use of $K(\beta)$. Section SI.III of the SI demonstrates how to generate a polynomial series expansion

of q_{st}^∞ ; the direct extrapolation of q_{st}^∞ did not consistently improve prediction of q_{st}^∞ over that based on eq 8. However, the direct extrapolation may prove beneficial when combined with an interpolation scheme that joins extrapolations at low and high temperature.

5 Summary and Conclusions

We have introduced a method for estimating the Henry’s law constant and low-pressure isosteric heat of adsorption as a function of temperature via extrapolation from direct calculations of those quantities at a single basis temperature. This extrapolation scheme is possible because the coefficients for a Taylor-series-based extrapolation of K_{H} and, thereby, q_{st}^∞ are simple to express (cf. eq 7) and may be rapidly computed using a Monte Carlo integration approach (Widom test particle insertion), which is itself essentially identical to the traditional method for computing K_{H} and q_{st}^∞ for a single T . Consequently, the extrapolation coefficients can be computed as part of a conventional K_{H} or q_{st}^∞ calculation with minimal extra computation, and thereby generating those important properties at other temperatures than the original basis temperature. Furthermore, existing molecular modeling toolkits have been adapted (FEASST) or could be adapted (RASPA is a likely candidate) to compute the coefficients, simply by adding new accumulators to the Widom routines. Our approach is valid for both crystalline and amorphous adsorbent materials provided that the material is rigid, since the relevant mathematical relationships rely on that constraint but make no other distinction or requirement of the nature of the adsorbent.

We presented extrapolation results for a simple test system (argon in a carbon nanotube represented by a smeared potential) and more complicated systems where the adsorbate and adsorbent are represented atomistically. The simple test system demonstrated the success of the extrapolation, for both K_{H} and q_{st}^∞ , under best-case conditions (essentially exact calculation of K_{H} , q_{st}^∞ , and K_j , hence no uncertainty in any of those quantities). The results showed that the extrapolation reproduced the directly calculated quantities, except for very

low temperatures, for an extrapolation based on a high basis temperature (T_0). The results also conform to mathematical expectations, namely that the extrapolation is most accurate when T_0 is near the midpoint of the desired T range, and the extrapolation’s range is only a limited distance in β space. The results for the Ar/MWCNT system suggest that a safe extrapolation range of at most 0.5 mol/kJ from the basis β_0 . Depending on β_0 or T_0 , this can correspond to many hundreds of kelvins. The more complicated adsorption systems (e.g., a MOF or zeolite with a small-molecule adsorbate) show qualitatively similar results to the simple test system, although subject to statistical uncertainty in K_j . In the demonstration MOF-adsorbate systems, the extrapolations of K_H and q_{st}^∞ were again successful for a high T_0 over a limited range of β ; the $|\beta - \beta_0| < 0.5$ mol/kJ range on β was similarly suggested as a range over which both K_H and q_{st}^∞ can be extrapolated reliably. The results of the test system also demonstrated the value of high-order extrapolation: The CO₂/ZIF-8 system showed that the extrapolation should use at least 10 coefficients, after which additional coefficients had little impact on the extrapolations. This observation is, however, subject to the caveat that uncertainty in the higher \overline{K}_j (which usually increases in relative terms with increasing j) may increase statistical uncertainty in the extrapolation without changing the extrapolation itself.

For additional validation of the extrapolation, we examined the extrapolation of K_H for the 11 660 adsorbent materials in the CoREMOF-2019 set by comparing the direct calculations of K_H with extrapolated estimates of \widehat{K}_H at 450 K and 600 K, where no system-specific adjustments were made to tune the calculations (which mimicks materials-screening exercises). The extrapolation reproduces the directly measured Henry’s law constant to within 10 % for the vast majority of materials. Materials for which K_H could not be extrapolated reliably were predominantly those materials with high K_H (greater than 10^{-1} mmol/kg/Pa) and/or those materials that failed to converge the extrapolation coefficients according to the desired convergence criteria. Thus, the study of this large set of materials adds another qualification for the extrapolation method: It is likely to work best when K_H itself is not

extremely large and when the coefficients are well converged. Lastly, the extrapolation is also able to predict nontrivial characteristics of adsorption systems, specifically that it accurately predicted the significant temperature dependence of the isosteric heat for a CO₂-zeolite system.

The extrapolation presented and implemented here is for systems with rigid adsorbents and rigid adsorbates, whereas adsorbates may be larger molecules whose bonds bend, stretch, or have dihedral rotations. K_H for nonrigid adsorbates is already known (cf. eq 1 of ref 18), but involves a ratio of the partition functions of a single adsorbate in the adsorbent and in an ideal gas state. Hence, an extrapolation for K_H for nonrigid adsorbates may in principle be derived similar to that presented here, but it will likely be more complex than the simple extrapolation in eqs 6 and 7. This will be addressed in future work.

In summary, we demonstrated how K_H and q_{st}^∞ may be estimated via extrapolation from a basis temperature T_0 by introducing an intermediary function (eq 5) that is easily expanded as a Taylor series in β . The extrapolation coefficients are straightforward to compute from the single-adsorbate potential energy by a suitable integration method (eq 7), and the number of coefficients that one chooses to compute is limited only by floating-point precision and desired convergence. Our results indicate that the extrapolation of either K_H or q_{st}^∞ may be quite accurate when the basis temperature is high and the extrapolation range is appropriately small in β space. Results for K_H suggest a range of $|\beta - \beta_0| < 0.5$ mol/kJ, while q_{st}^∞ is slightly more restricted to $|\beta - \beta_0| < 0.35$ mol/kJ; for both K_H and q_{st}^∞ we reiterate that the lower β (higher T) limit must be selected with caution to yield a sensible (positive) temperature. More importantly, this can correspond to hundreds of kelvins depending on T_0 . E.g., with $T_0 = 400$ K, an extrapolation range $\beta_0 - 0.15$ mol/kJ $< \beta < \beta_0 + 0.5$ mol/kJ is equivalent to 150 K $< T < 800$ K, hence, K_H and q_{st}^∞ could be estimated over a wide range of industrially relevant temperatures from a single calculation. Our extrapolation method may be added to existing suites of tools for screening adsorbent materials, such that screening exercises can simultaneously search for advantageous temperatures and materials

for a particular adsorption or separation application.

Supplementary Information

The Supplementary Information is available free of charge on publisher’s website at DOI: <https://pubs.acs.org/doi/10.1021/acs.jpcc.2c04583>.

I. Example Adsorption Systems: includes results from systems similar to the CO₂/ZIF-8 system, where the extrapolations are qualitatively similar to those in Figures 3 and 4. II. Uncertainty Estimation: derives the relationships necessary to estimate the uncertainty in direct calculations of K_H and q_{st}^∞ and in extrapolations of the same. III. Direct Extrapolation of q_{st}^∞ : derives an extrapolation of q_{st}^∞ itself, in contrast to the indirect extrapolation via $K(\beta)$. Results of the “direct” extrapolation are compared to results in Figures 2 and 4. IV. Padé Approximant: presents results for Padé Approximants based on the conventional Taylor Series extrapolation for the CO₂/ZIF-8 and CO₂/ITQ-29 systems. V. Example FEASST Scripts: shows how to compute extrapolation coefficients using FEASST and plots the results. The sample scripts can be used to recreate Figures 3 and 4.

Acknowledgments

The authors thank Dr. Peter Ravikovitch for clarifying that the sodalite cages of ITQ-29 were blocked in q_{st}^∞ calculations reported in ref 42.

Disclaimer

Official contribution of the National Institute of Standards and Technology; not subject to copyright in the United States of America. The authors declare no competing financial interest.

References

- (1) US Dept Energy Advanced Manufacturing Office, Bandwidth Study on Energy Use and Potential Energy Saving Opportunities in U.S. Petroleum Refining. 2015; https://www.energy.gov/sites/prod/files/2015/08/f26/chemical_bandwidth_report.pdf, Accessed: 6 June 2022.
- (2) National Academies of Sciences, Engineering, and Medicine, *A Research Agenda for Transforming Separation Science.*; The National Academies Press: Washington, DC, 2019.
- (3) Sholl, D. S.; Lively, R. P. Seven Separations to Change the World. *Nature* **2016**, *532*, 435–7.
- (4) Schoedel, A.; Ji, Z.; Yaghi, O. M. The role of metal–organic frameworks in a carbon-neutral energy cycle. *Nat Energy* **2016**, *1*, 16034.
- (5) Kreno, L. E.; Leong, K.; Farha, O. K.; Allendorf, M.; Duyne, R. P. V.; Hupp, J. T. Metal–Organic Framework Materials as Chemical Sensors. *Chem Rev* **2012**, *112*, 1105–1125.
- (6) Mallakpour, S.; Nikkhoo, E.; Hussain, C. M. Application of MOF materials as drug delivery systems for cancer therapy and dermal treatment. *Coordin Chem Rev* **2022**, *451*, 214262.
- (7) Zhou, H.-C.; Long, J. R.; Yaghi, O. M. Introduction to Metal–Organic Frameworks. *Chem Rev* **2012**, *112*, 673–674.
- (8) Matito-Martos, I.; Martin-Calvo, A.; Gutiérrez-Sevillano, J. J.; Haranczyk, M.; Doblare, M.; Parra, J. B.; Ania, C. O.; Calero, S. Zeolite screening for the separation of gas mixtures containing SO₂, CO₂ and CO. *Phys Chem Chem Phys* **2014**, *16*, 19884–19893.

- (9) Diercks, C. S.; Yaghi, O. M. The atom, the molecule, and the covalent organic framework. *Science* **2017**, *355*.
- (10) McKeown, N. B. Polymers of Intrinsic Microporosity (PIMs). *Polymer* **2020**, *202*, 122736.
- (11) Ongari, D.; Talirz, L.; Smit, B. Too Many Materials and Too Many Applications: An Experimental Problem Waiting for a Computational Solution. *ACS Central Sci* **2020**, *6*, 1890–1900.
- (12) Colón, Y. J.; Snurr, R. Q. High-throughput computational screening of metal–organic frameworks. *Chem Soc Rev* **2014**, *43*, 5735–5749.
- (13) Chung, Y. G.; Haldoupis, E.; Bucior, B. J.; Haranczyk, M.; Lee, S.; Zhang, H.; Vogiatzis, K. D.; Milisavljevic, M.; Ling, S.; Camp, J. S. et al. Advances, Updates, and Analytics for the Computation-Ready, Experimental Metal–Organic Framework Database: CoRE MOF 2019. *J Chem Eng Data* **2019**, *64*, 5985–5998.
- (14) Wilmer, C. E.; Leaf, M.; Lee, C. Y.; Farha, O. K.; Hauser, B. G.; Hupp, J. T.; Snurr, R. Q. Large-scale screening of hypothetical metal-organic frameworks. *Nat. Chem.* **2012**, *4*, 83–89.
- (15) Colón, Y. J.; Gómez-Gualdrón, D. A.; Snurr, R. Q. Topologically Guided, Automated Construction of Metal–Organic Frameworks and Their Evaluation for Energy-Related Applications. *Cryst Growth Des* **2017**, *17*, 4801–5810.
- (16) Willems, T. F.; Rycroft, C. H.; Kazi, M.; Meza, J. C.; Haranczyk, M. Algorithms and tools for high-throughput geometry-based analysis of crystalline porous materials. *Micropor and Mesopor Mater* **2012**, *149*, 134–141.
- (17) Sarkisov, L.; Bueno-Perez, R.; Sutharson, M.; Fairen-Jimenez, D. Materials Informatics with PoreBlazer v4.0 and the CSD MOF Database. *Chem Mater* **2020**, *32*, 9849–9867.

- (18) Sarkisov, L. Toward Rational Design of Metal-Organic Frameworks for Sensing Applications: Efficient Calculation of Adsorption Characteristics in Zero Loading Regime. *J Phys Chem C* **2012**, *116*, 3025–3033.
- (19) Yu, X.; Choi, S.; Tang, D.; Medford, A. J.; Sholl, D. S. Efficient Models for Predicting Temperature-Dependent Henry’s Constants and Adsorption Selectivities for Diverse Collections of Molecules in Metal–Organic Frameworks. *J Phys Chem C* **2021**, *125*, 18046–18057.
- (20) Sturluson, A.; Huynh, M.; Kaija, A.; Laird, C.; Yoon, S.; Hou, F.; Feng, Z.; Wilmer, C. E.; Colón, Y. J.; Chung, Y. G. et al. The role of molecular modeling and simulation in the discovery and deployment of metal-organic frameworks for gas storage and separation. *Mol Sim* **2019**, *45*, 1082–1121.
- (21) Choudhary, K.; Yildirim, T.; Siderius, D. W.; Kusne, A. G.; McDannald, A.; Ortiz-Montalvo, D. L. Graph neural network predictions of metal organic framework CO₂ adsorption properties. *Comp Mater Sci* **2022**, *210*, 111388.
- (22) Mahynski, N. A.; Blanco, M. A.; Errington, J. R.; Shen, V. K. Predicting low-temperature free energy landscapes with flat-histogram Monte Carlo methods. *J Chem Phys* **2017**, *146*, 074101.
- (23) Mahynski, N. A.; Errington, J. R.; Shen, V. K. Temperature extrapolation of multi-component grand canonical free energy landscapes. *J Chem Phys* **2017**, *147*, 054105.
- (24) Mahynski, N. A.; Jiao, S.; Hatch, H. W.; Blanco, M. A.; Shen, V. K. Predicting structural properties of fluids by thermodynamic extrapolation. *J Chem Phys* **2018**, *148*, 194105.
- (25) Mahynski, N. A.; Hatch, H. W.; Witman, M.; Sheen, D. A.; Errington, J. R.; Shen, V. K. Flat-histogram extrapolation as a useful tool in the age of big data. *Mol Sim* **2021**, *47*, 395–407.

- (26) Hatch, H. W.; Jiao, S.; Mahynski, N. A.; Blanco, M. A.; Shen, V. K. Communication: Predicting virial coefficients and alchemical transformations by extrapolating Mayer-sampling Monte Carlo simulations. *J Chem Phys* **2017**, *147*, 231102.
- (27) Monroe, J. I.; Hatch, H. W.; Mahynski, N. A.; Shell, M. S.; Shen, V. K. Extrapolation and interpolation strategies for efficiently estimating structural observables as a function of temperature and density. *J Chem Phys* **2020**, *153*, 144101.
- (28) June, R. L.; Bell, A. T.; Theodorou, D. N. Prediction of Low Occupancy Sorption of Alkanes in Silicalite. *J Phys Chem* **1990**, *94*, 1508–1516.
- (29) Huang, Y.-Y. The temperature dependence of isosteric heat of adsorption on the heterogeneous surface. *J Catal* **1972**, *25*, 131–138.
- (30) Widom, B. Some Topics in the Theory of Fluids. *J Chem Phys* **1963**, *39*, 2808–2812.
- (31) Hatch, H. W.; Mahynski, N. A.; Shen, V. K. FEASST: Free Energy and Advanced Sampling Simulation Toolkit. *J Res Natl Inst Stan* **2018**, *123*, 123004.
- (32) Dubbeldam, D.; Calero, S.; Ellis, D. E.; Snurr, R. Q. RASPA: molecular simulation software for adsorption and diffusion in flexible nanoporous materials. *Mol Sim* **2016**, *42*, 81–101.
- (33) Siderius, D. W.; Gelb, L. D. Extension of the Steele 10-4-3 potential for adsorption calculations in cylindrical, spherical, and other pore geometries. *J Chem Phys* **2011**, *135*, 084703.
- (34) Siderius, D. W.; Shen, V. K. Use of the Grand Canonical Transition-Matrix Monte Carlo Method to Model Gas Adsorption in Porous Materials. *J Phys Chem C* **2013**, *117*, 5861–5872.
- (35) Pérez-Pellitero, J.; Amrouche, H.; Siperstein, F. R.; Pirngruber, G.; Nieto-Draghi, C.; Chaplais, G.; Simon-Masseron, A.; Bazer-Bachi, D.; Peralta, D.; Bats, N. Adsorption

- of CO₂, CH₄, and N₂ on zeolitic imidazolate frameworks: Experiments and simulations. *Chem.-Eur. J.* **2010**, *16*, 1560–1570.
- (36) Bae, Y.-S.; Snurr, R. Q. Development and Evaluation of Porous Materials for Carbon Dioxide Separation and Capture. *Angew Chem Int Edit* **2011**, *50*, 11586–11596.
- (37) Potoff, J. A.; Siepmann, J. I. Vapor-liquid equilibria of mixtures containing alkanes, carbon dioxide, and nitrogen. *AIChE J.* **2001**, *47*, 1676–1682.
- (38) Zhang, H.; Snurr, R. Q. Computational Study of Water Adsorption in the Hydrophobic Metal–Organic Framework ZIF-8: Adsorption Mechanism and Acceleration of the Simulations. *J Phys Chem C* **2017**, *121*, 24000–24010.
- (39) Todorov, E. I.; Smith, W. “The DL_POLY User Manual” version 4.03. http://www.ccp5.ac.uk/DL_POLY/, Accessed 15 April 2022.
- (40) Rappe, A. K.; Casewit, C. J.; Colwell, K. S.; Goddard, W. A.; Skiff, W. M. UFF, a full periodic table force field for molecular mechanics and molecular dynamics simulations. *J Am Chem Soc* **1992**, *114*, 10024–10035.
- (41) Zou, C.; Penley, D. R.; Cho, E. H.; Lin, L.-C. Efficient and Accurate Charge Assignments via a Multilayer Connectivity-Based Atom Contribution (m-CBAC) Approach. *J Phys Chem C* **2020**, *124*, 11428–11437.
- (42) Hyla, A. S.; Fang, H.; Boulfelfel, S. E.; Muraro, G.; Paur, C.; Strohmaier, K.; Ravikovitch, P. I.; Sholl, D. S. Significant Temperature Dependence of the Isothermic Heats of Adsorption of Gases in Zeolites Demonstrated by Experiments and Molecular Simulations. *J Phys Chem C* **2019**, *123*, 20405–20412.
- (43) Pluth, J. J.; Smith, J. V. Accurate redetermination of crystal structure of dehydrated zeolite A. Absence of near zero coordination of sodium. Refinement of silicon,aluminum-ordered superstructure. *J Am Chem Soc* **1980**, *102*, 4704–4708.

- (44) Corma, A.; Rey, F.; Rius, J.; Sabater, M. J.; Valencia, S. Supramolecular self-assembled molecules as organic directing agent for synthesis of zeolites. *Nature* **2004**, *431*, 287–290.
- (45) Fang, H.; Kamakoti, P.; Ravikovitch, P. I.; Aronson, M.; Paur, C.; Sholl, D. S. First principles derived, transferable force fields for CO₂ adsorption in Na-exchanged cationic zeolites. *Phys. Chem. Chem. Phys.* **2013**, *15*, 12882–12894.
- (46) Gómez-Álvarez, P.; Ruiz-Salvador, A. R.; Hamad, S.; Calero, S. Importance of Blocking Inaccessible Voids on Modeling Zeolite Adsorption: Revisited. *J Phys Chem C* **2017**, *121*, 4462–4470.
- (47) Harris, J. G.; Yung, K. W. Carbon dioxide’s liquid-vapor coexistence curve and critical properties as predicted by a simple molecular model. *J Phys Chem* **1995**, *99*, 12021–12024.

TOC Graphic

